Progress In Electromagnetics Research Letters, Vol. 105, 121–129, 2022

Projection Constraint Null Broadening and Deepening Method for Conjugate Array

Shi-Jing Xiao, Bin Li*, and Qing Wang

Abstract—The performance of the Capon beamforming sharply decreases against strong directional and large deviation interference. In order to reduce the impact of the abnormal interference, this paper proposes a large degree of freedom null broadening beamforming for non-circular signals. The signal vector is first extended by a uniform linear conjugate array. The covariance matrix of the array is then reconstructed by projection transformation and diagonal loading technique. Finally, the beamforming is constrained by the characteristic subspace of the guide vector matrix, and the analytic expression of the optimal weights of the method is derived. The numerical simulations demonstrate that the proposed null broadening method has the advantages of high degrees of freedom and strong parameter selection robustness.

1. INTRODUCTION

Adaptive beamforming is widely used in radar, communication, sonar, and other fields because it adaptively adjusts the weight coefficients at the back end of each array element to form null in the direction of spatial interference, in order to ensure the expected signal without distortion [1–5]. In actual working conditions, the time-varying propagation environment, mechanical rotation of the receiving antenna, relative movement of the interference source and other factors make the interference angle not strictly fall on the deep and narrow zero trap. These spatial non-stationary characteristics lead to the mismatch between the training data and application data, which results in serious performance degradation [6–8]. The update rate of adaptive weights is constrained by the amount of chip computation and cannot be excessively improved. The null broadening technology is efficient in solving this problem [9].

In the early stage, null broadening is achieved using the Covariance Matrix Taper (CMT) technology by replacing the original single interference source angle with virtual spatial dense interference sources [10]. The adaptive diagonal loading CMT technology is used to deepen the zero-sink depth and increase the output signal-to-interference-noise ratio (SINR) [11]. The derivative constraint method achieves null broadening through multiple nulls constraint in one direction [12]. In [13], the first-order and second-order iterations make the main beam point at the desired signal and form a wide zero trap in the direction of the interference signal. However, this method cannot easily control the width of the null, and it has a low null depth. In [14], a method is developed using projection transformation (PT) of the data in order to reconstruct the covariance matrix. In addition, the approach proposed in [15] uses the linear constraint suppression (LCSS) of the optimal weight, which improves this problem. However, its performance decreases with the decrease of the number of interferences. The conjugated virtual array allows its virtual array elements to receive conjugated signals of mirror symmetric real array elements.

Received 11 May 2022, Accepted 14 July 2022, Scheduled 1 August 2022
* Corresponding author: Bin Li (libin521002@sina.com).
The authors are with the Department of National Key Laboratory of National Defense Technology for Integrated Ship Power Technology, Naval University of Engineering, Wuhan, China.

The simple structure efficiently increases the array aperture of non-circular signals, thus broadening the degree of freedom (DOF) of the array [16–18].

The main contribution of this paper is the proposition of a high DOF null broadening and deepening beamforming method, based on projective transformation with linear constraints in subspace of guide vector matrix (HD-PT-LC). The received arrays are first extended with a number of virtual conjugate sensors. A projection transformation is then performed on the received vector, and the covariance matrix is calculated after diagonal loading. Finally, the eigenspace of guide vector matrix is used to perform linear constraint on the weights of the adaptive beamforming. The beamformer can perform efficient null broadening and control of the null width. The conjugate array receiving method improves the contradiction that the increase of basis vector deepens the null depth and reduces the number of broadening interferences. The experimental results demonstrate that the proposed method can outperform several existing beamformers, in terms of strong angle mismatch, small snapshots, and strong parameter selection robustness.

2. THE PROPOSED CONSTRUCTION METHOD

The proposed method uses a virtual conjugate array to receive signals, combines projection transformation and diagonal loading to process the covariance matrix, and performs null broadening and deepening of weight constraints by characteristic subspace.

2.1. Date Expansion and Projection Transformation

Adaptive beamformer is shown in Fig. 1. Without loss of generality, a uniform linear array (ULA) with N element spacing of d is considered. There is one non-circular expectation signal from θ_0 and P non-circular interference signals from θ_k $(k = 1, 2, \ldots, P)$ incident to the array, whose envelops are $s_0(k)$ and $s_k(k)$ $(k = 1, 2, \ldots, P)$. The signal received by each array element can then be expressed as [19]:

$$x_n(t) = \mathbf{a}(\theta_s)s_0(t) + \sum_{k=1}^{P} \mathbf{a}(\theta_k)s_k(t) + n_n(t) \tag{1}$$

where the steering vector of uniform linear array is given by:

$$\mathbf{a}(\theta) = \left[1, e^{-j2\pi d \sin\theta/\lambda}, \ldots, e^{-j2\pi(N-1)d\sin\theta/\lambda}\right]^T \tag{2}$$

where $[.]^T$ is the envelope of a noncircular signal having the character of $s(t) = s^*(t)$; λ is the wavelength; $\mathbf{A} = [a(\theta_0), a(\theta_1), \ldots, a(\theta_P)]$ is the guiding vector matrix of the original array.

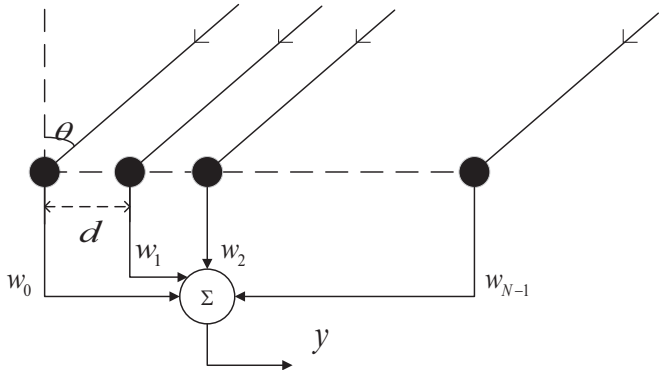

Figure 1. Adaptive beamformer.

The virtual conjugate uniform linear array model shown in Fig. 2 is designed by using the structural characteristics of the uniform linear array. The real array element and virtual array element are symmetrical with array element 0. The total number of array elements is $2N - 1$ after expansion.

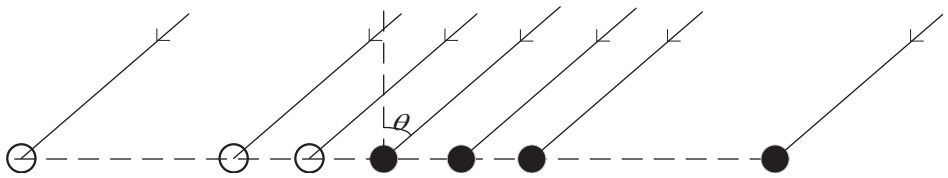

Figure 2. Uniform linear conjugate virtual array.

With the array element 0 as the reference array element, the received signal of the virtual array element $-n$ can be expressed as:

$$x_{-n}(t) = \mathbf{a}'(\theta_s)s_0(t) + \sum_{k=1}^{P} \mathbf{a}'(\theta_k)s_k(t) + n_{-n}(t) \tag{3}$$

where the steering vector of virtual uniform linear array is given by:

$$\mathbf{a}'(\theta) = \left[1, e^{-j2\pi(-d)\sin\theta/\lambda}, \ldots, e^{-j2\pi(N-1)(-d)\sin\theta/\lambda}\right]^T \tag{4}$$

The guidance vector of virtual array is the conjugate of the guidance vector of physical array. So the received signals of virtual array and physical array meet the equation:

$$x_{-n}(t) = x_n^*(t) \tag{5}$$

The expanded signal $\mathbf{X}(t) = [x_{1-N}(t), \ldots, x_0(t), \ldots, x_{N-1}(t)]^T$ received by the whole virtual conjugate linear array is expressed as:

$$\mathbf{X}(t) = \begin{bmatrix} \mathbf{JA}^* \\ \mathbf{A} \end{bmatrix} \mathbf{S}(t) + \begin{bmatrix} \mathbf{J} & \mathbf{0} \\ \mathbf{0} & \mathbf{I} \end{bmatrix} \begin{bmatrix} \mathbf{N}^*(t) \\ \mathbf{N}(t) \end{bmatrix} \tag{6}$$

where $\mathbf{I}$ is the identity matrix, and $\mathbf{J}$ is the antisymmetric matrix. The steer vector matrix received by the virtual conjugate array is given by:

$$\bar{\mathbf{A}} = \begin{bmatrix} JA^* \\ A \end{bmatrix} = [\bar{\mathbf{a}}(\theta_1), \ldots, \bar{\mathbf{a}}(\theta_k)] \tag{7}$$

where the steer vector matrix of the virtual conjugate array is expressed as:

$$\bar{\mathbf{a}}(\theta_k) = \left[e^{-j\frac{2\pi(1-N)d}{\lambda}\sin\theta_k}, \ldots, 1, \ldots, e^{-j\frac{2\pi(N-1)d}{\lambda}\sin\theta_k}\right]^T \tag{8}$$

The effective aperture of the array is expanded from N to $2N-1$, which efficiently broadens the DOF of the array.

Through prior estimation, the signal angle interval to be widened is Θ, and the guiding vector matrix in the interval is defined as:

$$\mathbf{R}_\theta = \int_\Theta \bar{\mathbf{a}}^H(\theta)\bar{\mathbf{a}}^H(\theta)d\theta \tag{9}$$

where $(.)^H$ denotes the Hermitian transpose operator.

Since $\mathbf{R}_\theta$ is a Hermite matrix, it is decomposed, and the eigenvector $\mathbf{u}_1, \mathbf{u}_2, \ldots, \mathbf{u}_L$ corresponding to L Large eigenvalues is used as the basis vector in order to form the eigen-subspace $\mathbf{U}_L$ of $\mathbf{R}_\theta$ as:

$$\mathbf{U}_L = span\{\mathbf{u}_1, \mathbf{u}_2, \ldots, \mathbf{u}_L\} \tag{10}$$

The basis vector in $\mathbf{U}_L$ is constructed as a projection operator:

$$\mathbf{T} = \sum_{k=1}^{L} \mathbf{u}_k\mathbf{u}_k^H \tag{11}$$

A projection transformation of the signal received by the virtual array is then performed:

$$\overline{\mathbf{X}} = \mathbf{TX} \tag{12}$$

Ideally, the signal subspace is orthogonal to the noise subspace. In practice, the array is affected by the number of snapshots and the signal propagation environment. Therefore, the orthogonality of signal subspace and noise subspace becomes worse, which results in a low beam performance [20, 21]. The projection transformation can improve the orthogonality of signal subspace and noise subspace. It can also improve the performance of the side lobe and deepen the depth of the null.

2.2. Linear Constraint Suppression

By limiting the output power in the widened area, the null is further deepened, that is, the weight vector $\mathbf{w}$ meets:

$$\mathbf{w}^H \mathbf{R}_\theta \mathbf{w} \leq \eta \Leftrightarrow \mathbf{w}^H \mathbf{U}_\theta \mathbf{\Lambda}_\theta \mathbf{U}_\theta^H \mathbf{w} \leq \eta \tag{13}$$

where η is a small positive number.

Under ideal conditions, the small eigenvalues of $\mathbf{R}_\theta$ are all zero. However, due to the influence of noise, number of snapshots, and other conditions, the small eigenvalues are generally not zero. Let the subspace $\mathbf{U}_L$ meet:

$$\mathbf{w}^H \mathbf{U}_L = 0 \tag{14}$$

It is important to mention that the increase of the number of basis vectors in subspace will weaken the impact of the small eigenvalues on the performance, so as to reduce the output power in the corresponding interval. Simultaneously, for each increase of basis vector, a linear constraint is added at the expense of one DOF [22].

2.3. Proposed Beamformer

In order to ensure the invertibility of the matrix, the artificially added noise ε is a small positive number. The reconstructed covariance matrix can be expressed as:

$$\overline{\mathbf{R}} = \frac{1}{K} \sum_{i=1}^{K} \overline{\mathbf{X}}_i(n) \overline{\mathbf{X}}_i^H(n) + \varepsilon \mathbf{I} \tag{15}$$

where K is the number of snapshots.

The desired direction is made with constant gain, and the feature subspace is used to linearly constrain the weight coefficient. The Lagrange multiplier function $L(\mathbf{w})$ is then constructed:

$$L(\mathbf{w}) = \mathbf{w} \overline{\mathbf{R}} \mathbf{w} + \left(\mathbf{w}^H \mathbf{P} - \mathbf{f} \right) \lambda + \lambda^H \left(\mathbf{f}^H - \mathbf{P}^H \mathbf{w} \right) \tag{16}$$

where constraint matrix $\mathbf{P} = [\mathbf{a}(\theta_0), \mathbf{U}_L]$ and constrained response matrix.

According to the solution conditions of Lagrange equation:

$$\begin{cases} \dfrac{\partial L(\mathbf{w})}{\mathbf{w}} = 0 \\ \mathbf{w}^H \mathbf{P} = \mathbf{f} \end{cases} \tag{17}$$

The solution of Eq. (13) yields the optimal beamformer given by:

$$\mathbf{w}_{opt} = \frac{\overline{\mathbf{R}} \mathbf{P} \mathbf{f}^H}{\mathbf{P}^H \overline{\mathbf{R}} \mathbf{P}} \tag{18}$$

The steps of the proposed method are shown in Table 1. The output signal to interference noise ratio (SINR) is expressed as:

$$\mathrm{SINR}_{out} = \frac{\sigma_0^2 \left| \mathbf{w}^H \mathbf{a}(\theta_0) \right|^2}{\mathbf{w}^H \left(\sum_{k=1}^{P} \sigma_k^2 \mathbf{a}\left(\theta_k\right) \mathbf{a}^H\left(\theta_k\right) + \sigma_n^2 \mathbf{I} \right) \mathbf{w}} \tag{19}$$

where σ_0^2 is the input expected signal power, σ_k^2 the input interference signal power, and σ_n^2 the noise power. Table 1 summarizes the steps of the proposed null broadening and deepening method.

Table 1. Summary of the proposed method steps.

Method: Linear Constrained Projection Transformation Null Broadening and Deepening of Conjugate Array
1: Input: for the reception vector $\mathbf{X}(t)$ of the uniform linear array, the widened null interval Θ is required and the incident direction of the desired signal is θ_0.
2: Initialization: diagonal loading ε; number of subspace basis vectors L.
3: Calculate steering vector matrix $\mathbf{R}_\theta = \int^{-H} \mathbf{a}(\theta)^{-H}\mathbf{a}(\theta)d\theta$.
4: Construct the characteristic decomposition matrix $\mathbf{R}_\theta$, and the characteristic subspace $\mathbf{U}_L$.
5: Calculate the projection transformation matrix $\mathbf{T} = \sum^{L} \mathbf{u}_k\mathbf{u}_k^H$.
6: Expand the vector matrix and perform projection transformation $\overline{\mathbf{X}}$= $\mathbf{TX}$.
7: Calculate the covariance matrix $\overline{\mathbf{R}} = \frac{1}{K}\sum_{i=1}^{K} \overline{\mathbf{X}}_i(n)\overline{\mathbf{X}}_i^H(n) + \varepsilon\mathbf{I}$.
8: Construct the constraint matrix $\mathbf{P} = [\mathbf{a}(\theta_0), \mathbf{U}_L]$ and constrained response matrix $\mathbf{f} = [1, 0, \ldots, 0]_{(L+1)\times 1}$.
9: Output: Calculate the best weight $\mathbf{w}_{opt} = \frac{\overline{\mathbf{R}}\mathbf{P}\mathbf{f}^H}{\mathbf{P}^H\overline{\mathbf{R}}\mathbf{P}}$.

3. SIMULATION AND PERFORMANCE ANALYSIS

In the simulation experiment, the array is the same omnidirectional uniform linear array. The array element spacing is half wavelength, and the signal and interference are independent of each other. The added noise is an independent Gaussian white noise. All the results are obtained from 100 independent Monte Carlo experiments. The common simulation $1 \sim 3$ parameters are shown in Table 2.

Table 2. Common simulation parameters.

Input Signal to Noise Ratio	0 dB
Input Interference to Noise Ratio	30 dB
θ_0	0°
ε	0.015
K	200

3.1. Simulation and Analysis of Angle Mismatch

The number of array elements, number of array elements of other comparison methods, incident angle of interference signal, and widening range are set to 6, 11, 40°, and $[36^\circ, 44^\circ]$, respectively. The number of basis vectors is 5. Fig. 3 shows the null broadening and deepening beamforming diagram of jamming signal for different methods, and the output SINR when the angle is mismatched.

It can be seen from Fig. 3 that the Minimum Variance Distortion Response (MVDR) beamformer has no null broadening, and the output SINR rapidly decreases in the case of angle mismatch, while the other methods widen the null. In the case of angle mismatch, the output SINR decreases very weakly, showing a certain robustness to angle mismatch. Due to the linear constraint on the weight vector as well as the projection transformation, the beamformer forms a deeper null and has a higher SINR than the comparison methods at the same mismatch angle.

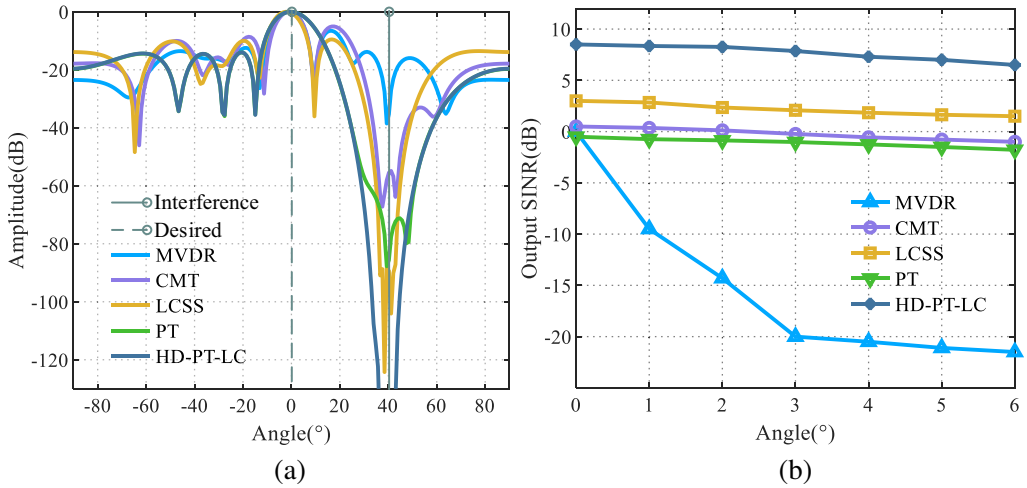

Figure 3. (a) Beam pattern of different methods. (b) Output signal to interference noise ratio under different mismatch angles. (Scenario 1: SNR = 0 dB, INR = 30 dB, $L = 5$, $K = 200$, $\varepsilon = 0.015$, $\theta_0 = 0°$, $\Theta = [36°, 44°]$).

3.2. Simulation and Analysis of Different Eigen-Subspace

In this section, the number of array elements is set to 6. That of the other comparison methods is set to 11. The incident angles of interference are $-30°$ and $40°$, and the widening interval of null is $[-32°, -28°] \cup [38°, 42°]$. The null broadening beam pattern generated by different methods, when the number of basis vectors is differently selected, is shown in Fig. 4.

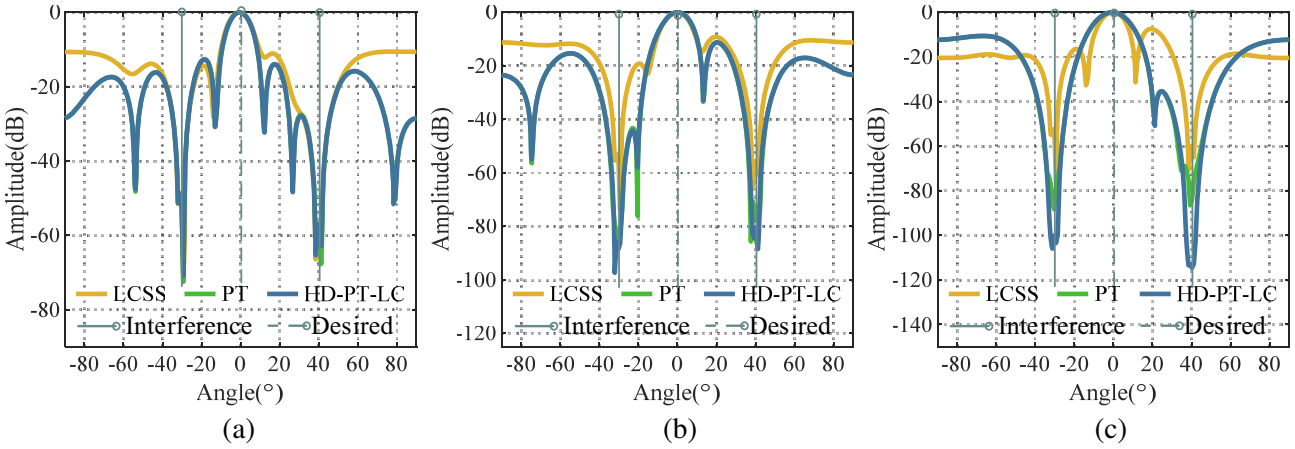

Figure 4. (a) Beam pattern of different methods when the number of basis vector is 4. (b) Beam pattern of different methods when the number of the basis vector is 6. (c) Beam pattern of different methods when the number of the basis vector is 8. (Scenario 2: SNR = 0 dB, INR = 30 dB, $L = 5$, $K = 200$, $\Theta = [-32°, -28°] \cup [38°, 42°]$, $\varepsilon = 0.015$, $\theta_0 = 0°$).

Combined with Fig. 3, the proposed method can efficiently control the null width. The null depth is deepened with the help of increasing the number of basis vectors. However, when the number of basis vectors is 4, the performances of Method [14], Method [15], and the proposed method are similar. With the increase of the basis vectors, the proposed method has a greater average null depth than the other two methods. As the number of basis vectors increases, the depth of the null and the width of the main lobe are greater. Moreover, the null broadening and deepening performance of the proposed method is

not lower than that of the LCSS and PT methods, regardless of the number of basis vectors. Therefore, the proposed method is robust to the selection of basis vectors. However, it requires to make a certain trade-off between the main lobe width and the null depth.

3.3. Simulation and Analysis of the Degree of Freedom

In this section, the linear constrained projection method without virtual array reception (PT-LC), HD-PT-LC and the traditional MVDR method are compared. The number of array elements is 5. When the incoming wave direction of the array subjected to two interferences is respectively $-30°$ and $60°[-32°, -28°] \cup [58°, 62°]$ is the widening interval. Fig. 5(a) shows the simulation results when the number of basis vectors is 3. The beamforming patterns of the proposed method for numbers of basis vectors of 3 and 5 are compared when the conjugate virtual array expands the degree of freedom from N to $2N-1$. Fig. 5(b) shows the obtained result.

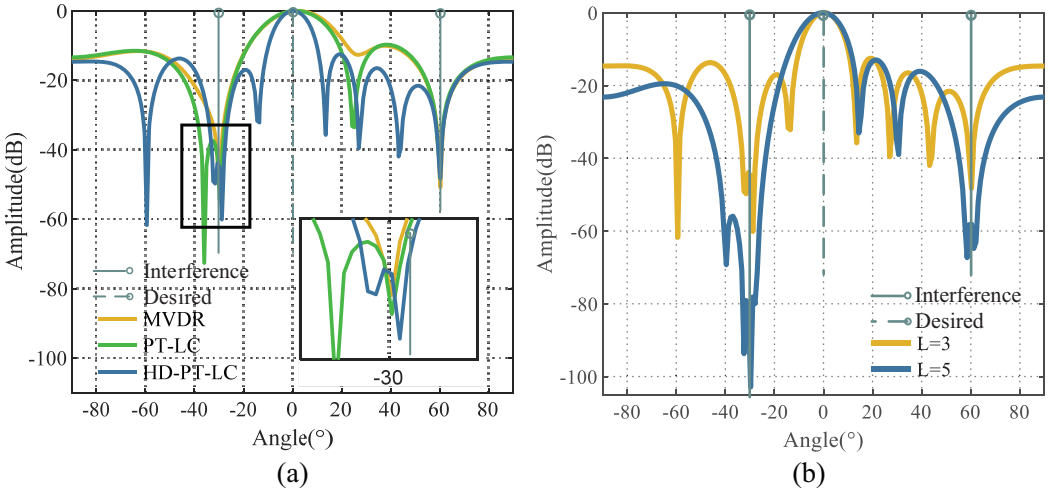

Figure 5. (a) Beam pattern of different methods when the number of interferences is 4 with the number of basis vector $L = 3$. (b) Beam pattern of HD-PT-LC when the number of basis vectors is 3 and 5. (Scenario 3: $N = 5$, SNR $= 0$ dB, INR $= 30$ dB, $\Theta = [-32°, -28°] \cup [58°, 62°]$, $K = 200$, $\varepsilon = 0.015$, $\theta_0 = 0°$).

It can be seen that the minimum number of effective apertures that the beamformer needs in order to achieve effective broadening should be 6 when the sensors receive 2 interferences, and the number of basis vectors is 3. At this time, the DOF of PT-LC array is not enough, and the MVDR method can form a null in the incident direction of the set interference signal. HD-PT-LC has only one null widening with the PT-LC method, due to the small number of basis vector selection. However, the null widening interval of the HD-PT-LC method is more accurate than that of the PT-LC method. The deepest null widening interval obtained by PT-LC is left relative to the required one, and its widening interval is not accurate. On the contrary, HD-PT-LC nearly doubles the base vector. When the number of base vectors is changed to 5, an effective null broadening and deepening can be formed in the required area. Significantly, HD-PT-LC has a narrower main lobe width and lower side lobe level than PT-LC, which makes the proposed beamformer have a better beam directivity and higher output SINR.

3.4. Simulation and Analysis of the Parameter Robustness

In this section, the simulation parameters are similar to those in Section 3.1, except for the number of snapshots and diagonal loading coefficient. The beam pattern of the proposed method is shown in Fig. 6(a) when the numbers of snapshots are 20, 200, and 2000. Fig. 6(b) shows the results when the diagonal loading coefficients are 0.15, 0.015, and 0.0015.

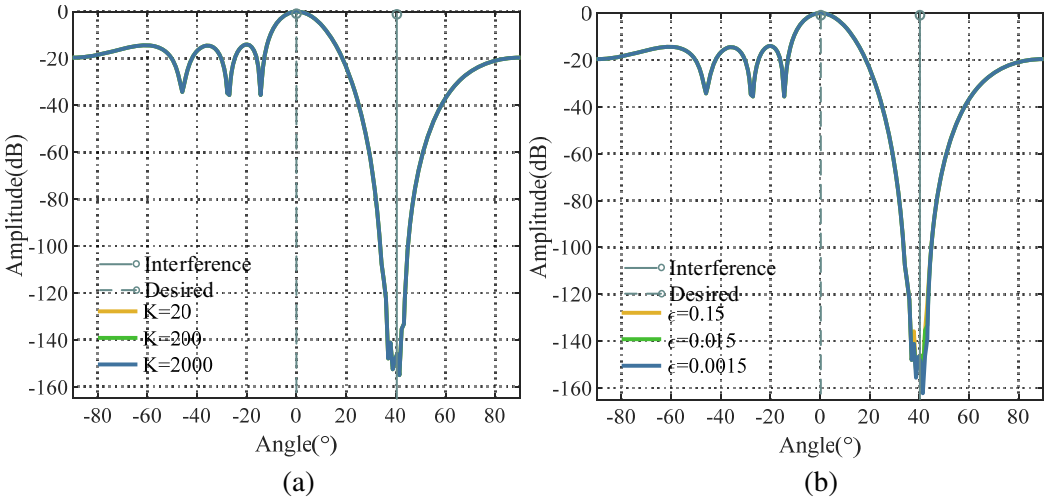

Figure 6. (a) Beam pattern of HD-PT-LC methods under snapshots. (b) Beam pattern of HD-PT-LC methods under different added noise. (Scenario 4: SNR = 0 dB, INR = 30 dB, $L = 5$, $\theta_0 = 0°$, $\Theta = [36°, 44°]$).

It can be seen from Fig. 6 that the beam patterns of the proposed method mainly coincide when the numbers of snapshots are 20 and 2000, and can still have a good null broadening and deepening effect under very low snapshots. The beam patterns with diagonal loading values in the interval $[0.0015, 0.15]$ are also mainly coincident. Thus, the proposed method has strong robustness in parameter selection, and it is suitable for engineering applications.

4. THE PROPOSED CONSTRUCTION METHOD

In this paper, the problem of the performance degradation of beamformer caused by the rapid change of interference incident angle is studied. A null broadening and deepening method, based on projection transformation and linear constraint on the received data of conjugate linear array, is proposed. The results of the simulations demonstrate that the proposed method has the performance characteristics of controllable null width, deep null, high degree of freedom, and strong parameter robustness. Finally, the proposed approach can be used for three-dimensional beamforming, and extended for engineering applications.

REFERENCES

1. Jian, L. and S. Petre, *Robust Adaptive Beamforming*, John Wiley & Sons, Inc., 2005.
2. Chen, X., T. Shu, K.-B. Yu, J. He, and W. Yu, "Joint adaptive beamforming techniques for distributed array radars in multiple mainlobe and sidelobe jammings," *IEEE Antennas and Wireless Propagation Letters*, Vol. 19, No. 2, 248–252, 2019.
3. Chen, X., et al., "Magnetic metamirrors as spatial frequency filters," *IEEE Transactions on Antennas and Propagation*, Vol. 68, No. 7, 5505–5511, 2020.
4. Sohrabi, F., Z. Chen, and W. Yu, "Deep active learning approach to adaptive beamforming for mmwave initial alignment," *IEEE Journal on Selected Areas in Communications*, Vol. 39, No. 8, 2347–2360, 2021.
5. Bi, Y., "Robust adaptive beamforming based on interference-plus-noise covariance matrix reconstruction method," *Progress In Electromagnetics Research M*, Vol. 97, 87–96, 2020.
6. Zhang, M., A. Zhang, and Q. Yang, "Robust adaptive beamforming based on conjugate gradient algorithms," *IEEE Transactions on Signal Processing*, Vol. 64, No. 22, 6046–6057, 2016.

7. Huang, Y., S. A. Vorobyov, and Z.-Q. Luo, "Quadratic matrix inequality approach to robust adaptive beamforming for general-rank signal model," *IEEE Transactions on Signal Processing*, Vol. 68, 2244–2255, 2020.
8. Salvati, D., C. Drioli, and G. L. Foresti, "A low-complexity robust beamforming using diagonal unloading for acoustic source localization," *IEEE/ACM Transactions on Audio, Speech, and Language Processing*, Vol. 26, No. 3, 609–622, 2018.
9. Yang, H., P. Wang, and Z. Ye, "Robust adaptive beamforming via covariance matrix reconstruction under colored noise," *IEEE Signal Processing Letters*, Vol. 28, 1759–1763, 2021.
10. Guerci, J. R., "Theory and application of covariance matrix tapers for robust adaptive beamforming," *IEEE Transactions on Signal Processing*, Vol. 47, No. 4, 977–985, 1999.
11. Pajovic, M., J. C. Preisig, and A. B. Baggeroer, "Analysis of optimal diagonal loading for MPDR-based spatial power estimators in the snapshot deficient regime," *IEEE Journal of Oceanic Engineering*, Vol. 44, No. 2, 451–465, 2018.
12. Pan, C., J. Benesty, and J. Chen, "Design of directivity patterns with a unique null of maximum multiplicity," *IEEE/ACM Transactions on Audio, Speech, and Language Processing*, Vol. 24, No. 2, 226–235, 2015.
13. Ors, B. and R. Suleesathira, "First and second order iterative null broadening beamforming," *2019 3rd International Conference on Imaging, Signal Processing and Communication (ICISPC)*, 47–51, 2019, IEEE.
14. Landon, J., B. D. Jeffs, and K. F. Warnick, "Model-based subspace projection beamforming for deep interference nulling," *IEEE Transactions on Signal Processing*, Vol. 60, No. 3, 1215–1228, 2011.
15. Somasundaram, S. D., "Linearly constrained robust Capon beamforming," *IEEE Transactions on Signal Processing*, Vol. 60, No. 11, 5845–5856, 2012.
16. Li, S. and X.-P. Zhang, "Dilated arrays: A family of sparse arrays with increased uniform degrees of freedom and reduced mutual coupling on a moving platform," *IEEE Transactions on Signal Processing*, Vol. 69, 3367–3382, 2021.
17. Li, J., J. Zhao, Y. Ding, Y. Li, and F. Chen, "An improved co-prime parallel array with conjugate augmentation for 2-D DOA estimation," *IEEE Sensors Journal*, Vol. 21, No. 20, 23400–23411, 2021.
18. Song, J., F. Shen, and J. Shen, "Sparse array design exploiting the augmented conjugate correlation statistics for DOA estimation," *IEEE Access*, Vol. 8, 41951–41960, 2020.
19. Shaw, A., J. Smith, and A. Hassanien, "MVDR beamformer design by imposing unit circle roots constraints for uniform linear arrays," *IEEE Transactions on Signal Processing*, Vol. 69, 6116–6130, 2021.
20. Wax, M. and A. Adler, "Subspace-constrained array response estimation in the presence of model errors," *IEEE Transactions on Signal Processing*, Vol. 69, 417–427, 2020.
21. Wax, M. and A. Adler, "Detection of the number of signals by signal subspace matching," *IEEE Transactions on Signal Processing*, Vol. 69, 973–985, 2021.
22. Zheng, Z., W.-Q. Wang, Y. Kong, and Y. D. Zhang, "MISC array: A new sparse array design achieving increased degrees of freedom and reduced mutual coupling effect," *IEEE Transactions on Signal Processing*, Vol. 67, No. 7, 1728–1741, 2019.